Pattern formation and spatiotemporal chaos in the presence of boundaries

Stefan Rudroff and Ingo Rehberg
Otto-von-Guericke-Universität, Institut für Experimentelle Physik, Postfach 4120, D-39016 Magdeburg, Germany
(Received 6 August 1996)

Experimentally obtained time averages of disordered spatiotemporal chaotic patterns of electroconvection in a nematic liquid crystal reveal an ordered structure due to the boundaries of the pattern-forming system. The instantaneous snapshots and the time averages are characterized in terms of amplitude, wave number, and correlations in space and time. The averages have a significantly larger correlation length than that of the snapshots. Time averages reveal a wave number that differs from that of the underlying snapshots. Quantization effects within the regime of spatiotemporal chaos are found for the correlation length and for the estimated angle of coherent zigzag structures. [S1063-651X(97)02003-5]

PACS number(s): 47.52.+j

I. INTRODUCTION

Pattern formation is a subdivision of nonlinear dynamics, where spatial and temporal uniform systems lose stability under an external stress and patterns with periodic or chaotic behavior in space and time arise. While the mechanism of pattern formation is reasonably well understood within the framework of linear and weakly nonlinear theories, the spatiotemporal chaos (STC) arising sufficiently far above threshold is the subject of current investigations.

We define STC with reference to [1,2] as a dynamic system with an extensive number of degrees of freedom but with a remaining characteristic wave number. This definition separates STC from a periodic state on the one hand, and a turbulent state on the other hand. Surely, the transition from STC to turbulence is continuous, but the tools that are good for analyzing fully developed turbulence neglect the existence of a characteristic wavelength [3] and are thus not suitable for STC.

The purpose of this paper is to describe a special property of spatiotemporal chaos in the presence of boundaries. According to recent works [4–6], time averages of spatially confined STC reveal a higher degree of order than instantaneous snapshots. While these experiments deal with isotropic systems, we investigate spatially confined STC in an anisotropic system, namely, electroconvection (EC) in a nematic liquid crystal [7,8] (see Fig. 1). Then the patterns that arise have D_2 symmetry. To quantify the amount of order, we describe the patterns in terms of amplitude, wave number, and correlations in space and time. The spatial correlation length is then regarded as a measure of the degree of order of the patterns. Because we perform EC in a rectangular convection cell, there are, with respect to the D_2 symmetry, two kinds of boundary conditions that either support [9,10] or suppress [11] pattern formation. Their influence on the onset and stability of convection is studied as well.

II. EXPERIMENTAL SETUP AND PROCEDURE

A. Experimental setup

Electroconvection is an electrically driven instability in a thin layer of a nematic liquid crystal leading to more-or-less ordered patterns. We use the standard material 4-methoxygenzlidene-4′-*n*-butylaniline and visualize these patterns with a microscope and a charge-coupled-device camera using the standard experimental setup [7,12].

In our case, EC takes place between two crossed stripes of InO, which form a square capacitor with a volume of $550\times550\times24\ \mu\mathrm{m}^3$. The stripes are created from an InO-coated glass by a corrosive technique. The spacing $d=24\ \mu$m between the plates determines the wavelength of the EC pattern. All lengths presented below are scaled with this number. A mechanical treatment of the surface fixes the orientation (director) of the anisotropic nematic liquid crystal in a defined direction parallel to the surface of the glass (planar orientation) and defines the x axis. The stationary periodic pattern is then perpendicular to this direction.

The image of the $550\times550\ \mu\mathrm{m}^2$ convection cell is digitized by 352×512 pixels with 256 gray steps. These data are reduced to a 256×256 array of bytes by software and rescaled with a previously measured unstructured ground state I_0,

$$K(\mathrm{row,col})=128\frac{I(\mathrm{row,col})}{I_0(\mathrm{row,col})},$$

to compensate for inhomogeneous illumination and rescale

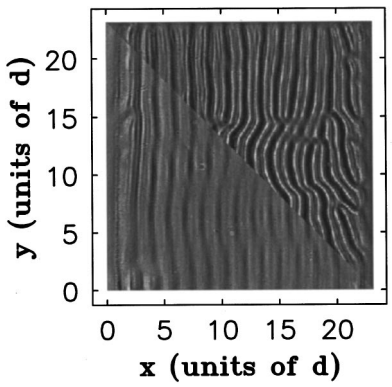

FIG. 1. Average (bottom left) and snapshot (top right) of spatiotemporal chaotic patterns taken from electroconvection in a finite cell. The average consists of 1024 snapshots at 8 V and 10 Hz. This corresponds to a control parameter of $\epsilon=0.66$.

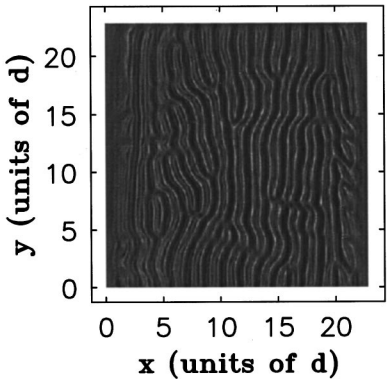

FIG. 2. Snapshot of a STC pattern at $\epsilon = 0.66$. The picture shows the entire convection cell [550×550 μm^2 ($23d \times 23d$)].

intensity. Then, K is rounded to an integer and stored again in an array of 256×256 bytes for reasons of computational efficiency.

B. Numerical data handling

One quantity used to characterize STC is the degree of translational invariance (correlation length) of a row or a column of a digitized image of the pattern. This image can either be a snapshot of the pattern (Fig. 2) or represent the temporal development of one horizontal line at $y = 11.5d$, which we call spatiotemporal (ST) image (see Fig. 3). Finally, the image can be an arithmetical mean (average) of many snapshots (Fig. 4).

All three kinds of images show similar structures, which can be analyzed by the same algorithm. This algorithm calculates a structure function

$$S(m) = \frac{1}{128} \sum_{n=0}^{127} [K(n) - K(n+m)]^2 \quad \text{with} \quad m = 0, \ldots, 127$$

from a row (or a column) of the rescaled digitized image. The structure function contains the same information as the autocorrelation, but can be calculated much faster by using a lookup-table technique. By averaging all columns (or rows) we get the following structure functions:

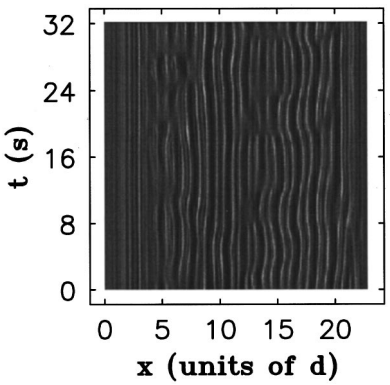

FIG. 3. Space-time plot (ST image) of a STC pattern at $\epsilon = 0.66$.

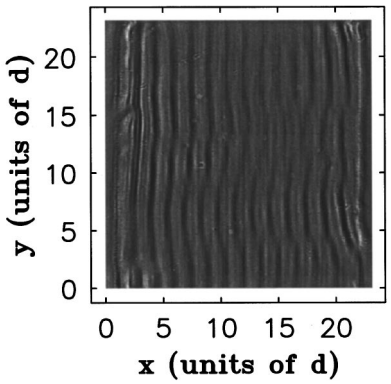

FIG. 4. The average of 1024 snapshots of a STC pattern at $\epsilon = 0.66$.

Orientation	Snapshot	ST-image	Average
$\langle S(\Delta\text{col})\rangle_{\text{row}}$	$\langle S(\Delta x)\rangle_y$	$\langle S(\Delta x)\rangle_t$	$\langle S(\Delta x)\rangle_y$
$\langle S(\Delta\text{row})\rangle_{\text{col}}$	$\langle S(\Delta y)\rangle_x$	$\langle S(\Delta t)\rangle_x$	$\langle S(\Delta y)\rangle_x$

where $\langle\ \rangle$ denotes the average.

Based on these structure functions, the characteristic parameters amplitude, wave number, correlation time, and correlation length are determined by a fit [13]. The fit functions are

$$S(\Delta x) = S_{\text{off}} - [A\cos(k\Delta x) + B\sin(2k\Delta x)]e^{-(\Delta x/\xi)^2},$$

$$S(\Delta t) = S_{\text{off}} - Ce^{-(\Delta t/\tau)^2}.$$

The Gaussian-shaped decay is phenomenologically motivated. It fits the data better than a pure exponential decay and takes care of the reflection symmetry of the structure function with respect to the origin. In particular, we extract the amplitude A, the wave number k, and the correlation length ξ from $\langle S(\Delta x)\rangle_y$ and the correlation time τ from $\langle S(\Delta t)\rangle_x$. The offset S_{off} is needed as an additional fit pa-

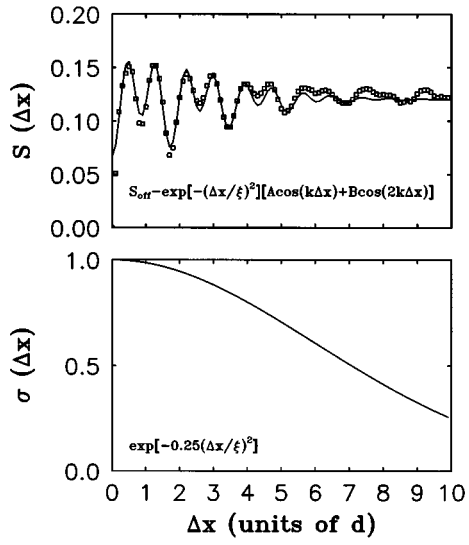

FIG. 5. Fit to the structure function $S(\Delta x)$ of the pattern shown in Fig. 2. The lower plot displays the significance with which the data are considered by the fit.

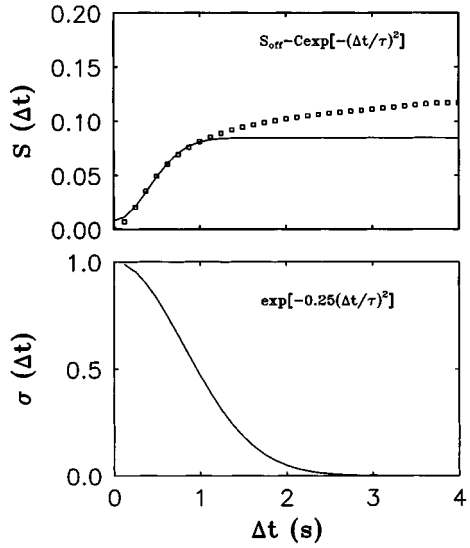

FIG. 6. Fit to the structure function $S(\Delta t)$ of the pattern shown in Fig. 3. The lower plot again displays the significance with which the data are considered by the fit.

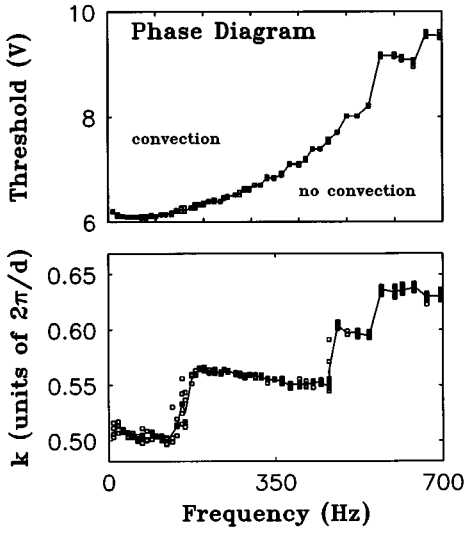

FIG. 7. Phase diagram: the threshold and the wave number k at the onset of convection within a finite cell.

rameter. It provides a measure for uncorrelated noise of the experimental setup and thus does not contain any relevant information.

Examples of the fitted structure functions in the regime of STC are shown in Figs. 5 and 6. Technical features of the fit are that it neglects the first data point $S(0)$ with regard to the uncorrelated noise of the experimental setup and there is an individual significance $\sigma(m)$, with which the data are considered by the fitting procedure. Data points close to the origin are given a high significance compared to those data points that are beyond the correlation length ξ and the correlation time τ. We adapt the significance $\sigma(m)$ of the values $S(m)$ within an iterative process to the previously fitted values of ξ and τ: $\sigma(m)=e^{-(m/4\xi)^2}$ or $\sigma^{-(m/4\tau)^2}$. Although we use empirical functions that do not fit the structure function for large lag data perfectly, this concept of an iterative fit with an adaptive significance gives reproducible values of the fit parameters in question.

III. EXPERIMENTAL RESULTS

A. Onset of convection in a finite cell

To measure the critical voltage V_c for the onset of convection, we fix the frequency and approach the threshold from subcritical values of the voltage by increasing the voltage in certain steps. We start with a voltage of 5 V and a step width of 1 V. After each step, we let the system relax 30 s and then a snapshot of the central 80% of the pattern in the convection cell is taken and analyzed. When the amplitude A passes a fixed value corresponding to a supercritical control parameter $\epsilon=(V^2-V_c^2)/V_c^2$ of about 0.5%, we decrease the voltage one step and bisect the step width. The process is stopped when a desired precision of 0.01 V for the threshold is achieved. This is repeated five times for each frequency. Figure 7 shows the threshold V_c and the critical wave number k_c as function of the frequency.

As shown in [14,15] in infinite cells, V_c and k_c are continuously increasing functions of the frequency. In our case, the box quantization leads to discontinuous jumps of the critical wave number, which are accompanied by discontinuities of the threshold voltage.

The plateaus, where the wave number is almost constant, have a local tendency towards smaller wave numbers for increasing frequency. This is not in contradiction to the wave-number quantization because the measurement of the wave number is restricted to the central 80% of the convection cell. It means that the pattern in the center is stretched, while the local wave number near the boundaries follows the global tendency to become larger for increasing frequency. Imperfect bifurcation within our system may be regarded as the likely relevant explanation for this effect. At control parameter values near threshold, the boundaries force a higher amplitude of convection in their vicinity compared to the amplitude of convection in the center of the cell. The wave number of this higher amplitude convection is closer to the critical wave number of the infinite system [16], which increases with increasing frequency for EC. With respect to the box quantization effects in our finite cell, an increase of the wave number near the boundaries will force a decrease of the wave number in the center of the convection cell, where the data of Fig. 7 are acquired. In addition, it seems worth mentioning that measurements of average patterns of capillary ripples show the same wave-number–frequency dependence in the regime of STC [4], although the underlying physics will be completely different.

B. Hysteresis of box quantized wave numbers

Figure 8 shows the wave number k of the pattern and its corresponding order parameter Θ as a function of the driving voltage and a frequency of 10 Hz. Θ is calculated according to [12]

$$\Theta=0.61\frac{2\pi}{kd}\sqrt{A}.$$

This value is proportional to the director distortion for sufficiently small values of the order parameter and is usually

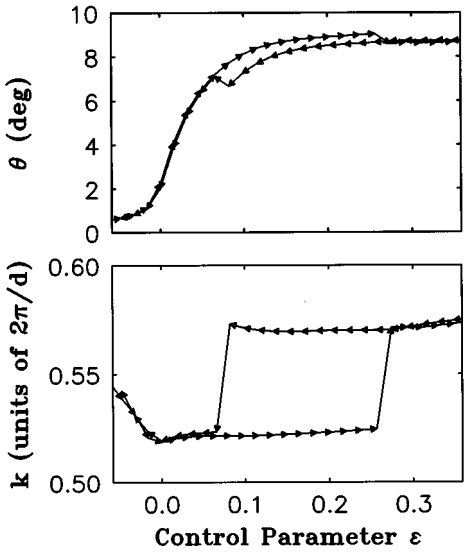

FIG. 8. Order parameter Θ and wave number k for increasing and decreasing control parameters in the regime of stationary periodic patterns.

regarded as the natural order parameter of the EC system. In our working regime the proportionality between A and Θ^2 is no longer valid, but we can at least expect a monotonic relation between our order parameter and the director distortion.

In Fig. 8 there is a subcritical pattern due to an imperfect bifurcation induced by the lateral boundaries that support pattern formation [9,10]. Nevertheless, we determine the threshold by assuming a perfect bifurcation and extrapolating the expected quadratic growth of the amplitude near the threshold. A discontinuous jump of the wave number and the existence of a hysteresis for stationary periodic patterns is clearly demonstrated. The subcritical patterns show a continuous change of wave number. We believe that this is caused by the influence of the imperfect bifurcation, which provides a finite amplitude at the lateral boundaries and a strong spatial modulation of amplitude and wave number, especially in the subcritical regime. When increasing the control parameter to the threshold the amplitude will become more homogeneous througout the convection cell, and this will lead to a more homogeneous wave number that has to match the box size. In the case of Figs. 8 and 9, this adjustment process corresponds to a decrease in the wave number in the bulk.

For illustration, we embed the experimental data in an *ad hoc* stability diagram (Fig. 9), which is based on numerical

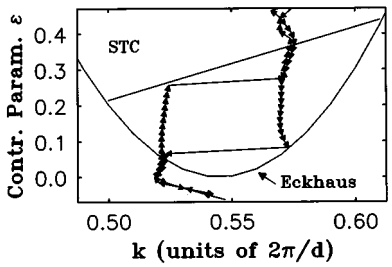

FIG. 9. Data of Fig. 8 in an *ad hoc* stability diagram for an infinite EC system.

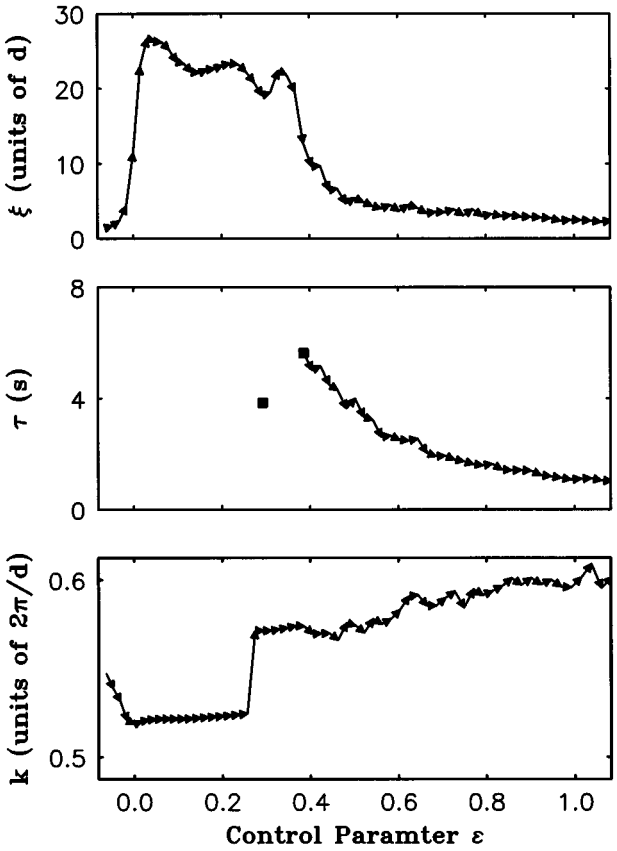

FIG. 10. Wave number k, correlation length ξ, and correlation time τ of the snapshots as a function of increasing control parameter.

stability diagrams for an infinite EC system [17]. We interpret the discontinuous jump at $\epsilon = 0.07$ as being a result of the Eckhaus instability [11,17–20] in our finite system. The jump at $\epsilon = 0.25$ is a result of a secondary instability of the normal rolls. We have not made any attempt to identify this instability. When comparing with Ref. [17], the zigzag instability seems to be the most natural interpretation. We note, however, that our instability occurs at a value of the control parameter that is about a factor of 10 larger than the theoretical estimate, but is in agreement with other experimental investigations [15,18]. It seems reasonable to assume that our lateral boundaries suppress the zigzag instability. A theoretical calculation of secondary instabilities for a low-aspect-ratio rectangular cell is not available at the moment.

C. Route to spatiotemporal chaos

In Fig. 10 we show the wave number k, correlation length ξ, and correlation time τ as a function of the driving ac voltage at a frequency of 10 Hz. The voltage range from 6 V to 9 V (theshold 6.2 V) is scanned up and down ten times by steps of 0.01 V. After each step, the system is allowed to relax 300 s and one ST image, one snapshot, and one average are taken and stored. The ST image covers a time interval of 32 s and the average consists of 64 snapshots taken 1.3 s apart. In total we measured 150 h. This gives 3600 stored images. During this time, the temperature is held constant to $15.0\,^{\circ}\mathrm{C} \pm 0.1\,^{\circ}\mathrm{C}$.

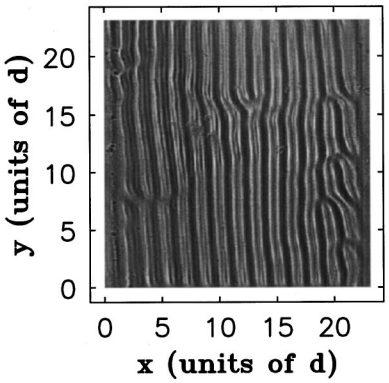

FIG. 11. Snapshot at ($\epsilon=0.4$) with a defect structure at the left lateral boundary.

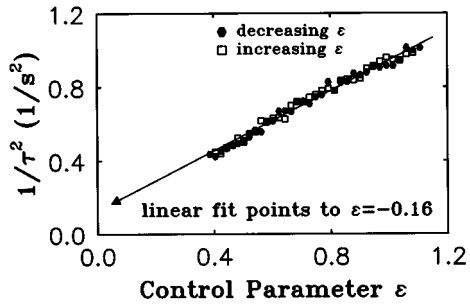

FIG. 12. Correlation time τ of ST images for increasing (squares) and decreasing (circles) control parameters.

To analyze the data set, the structure functions of the ten images corresponding to the same voltage and scanning direction are averaged. Then the relevant parameters are calculated by the fit to the autocorrelation. The results for increasing control parameter are shown in Fig. 10.

If there is no detectable motion in the system, the fit to the temporal autocorrelation will lead to meaningless values of the correlation time τ. In this case, our algorithm would focus on correlation times given by the camera noise and other fluctuations in the experimental setup, which must be considered as artifacts of the measurement and are thus omitted in Fig. 10.

The first striking point is a discontinuity of the wave number at $\epsilon\approx0.3$ accompanied by a finite correlation time τ of about 4 s, which indicates a time-dependent pattern. This time dependence is, however, only a transient due to an insufficient relaxation time after the voltage has been increased. The transition from one box quantized wave number to another is mediated by the creation and annihilation of defects occurring on time scales beyond the relaxation time of 300 s.

The second point is the abrupt onset of irregular motion at $\epsilon\approx0.4$, indicated by a finite correlation time $\tau\approx6$ s. The decrease of correlation time is accompanied by a decreasing correlation length. It is an interesting feature that the correlation length ξ clearly falls below the system size $L=23d$ when STC arises in the system.

Third, we note that, in contrast to Fig. 7, local and global tendencies of the wavelength measured in the center of the cell are now identical. The wave number increases with increasing voltage. It turns out that the corresponding increase of wavelength at the boundaries leads to an unstable pattern and defects are created mainly at the lateral boundaries, as indicated in Fig. 11.

In Fig. 10 the onset of spatiotemporal chaos at $\epsilon\approx0.4$ is indicated by a discontinuous jump to a finite correlation time $\tau\approx6$ s. To answer the ensuing question about a hysteresis at the onset of STC, we measure the correlation times for increasing and decreasing voltage. The results are shown in Fig. 12. There is no hysteresis within the experimental resolution. For capillary ripples, a similar discontinuous jump without hysteresis was already reported in Ref. [6], while a continuous transition to STC was found in Ref. [21]. In another EC experiment, the transition to STC seems to show a hysteresis [22].

The typical correlation time of the chaotic system seems to follow a power law $\tau(\epsilon)\sim(\epsilon-\epsilon_d)^{-0.5}$, with $\epsilon_d\approx-0.16$. This empirical finding is similar to results of Ref. [21], where a characteristic frequency of pattern fluctuations was measured, yielding an exponent of 0.5.

We can only speculate about the meaning of ϵ_d. It might indicate the lower boundary of the range of existence of the STC attractor. The range $\epsilon_d<\epsilon<0.4$ would be the range of coexistence of two different attractors, namely, STC and ordered patterns for $0<\epsilon<0.4$, and STC and the unstructured ground state for $\epsilon_d<\epsilon<0$. While coexistence of STC with an ordered state is known from spiral defect chaos [23], the coexistence of a STC state with the unstructured ground state would seem more unusual.

D. Time averages

In recent experiments, time averages of STC patterns with a high degree of order compared to instantaneous snapshots were found [4–6]. In contrast, we deal with an anisotropic fluid. Thus the averages do not keep the symmetry of the container, but rather show the reduced D_2 symmetry, which in our case is produced by the anisotropic fluid. Figure 4 displays an example of a time average of 1024 snapshots, taken from our experiment at $\epsilon=0.66$ and $f=10$ Hz. This average was created in 1400 s, which corresponds to 700 correlation times τ for the chosen control parameter. So the snapshots creating the average are uncorrelated.

1. Correlations and amplitudes

In Fig. 13 we show the order parameter Θ and the correlation length ξ of snapshots and averages, determined from the entire pattern (100% of the cell). This means that the data include the local parameter values of the boundary layer as well as those of the central regime of the convection cell. As can be seen in Fig. 13, there is a difference between snapshots and averages for $\epsilon>0.4$. In this range of the control parameter, STC takes place. Here the averages have a lower contrast and a higher degree of order compared to the individual snapshots. In terms of our fit parameters, the contrast is represented by the order parameter Θ and the amount of order is described by the correlation length ξ. For a moderate value of the control parameter within the regime of STC ($\epsilon\approx1$), the correlation length of the average is twice the correlation length of the snapshots.

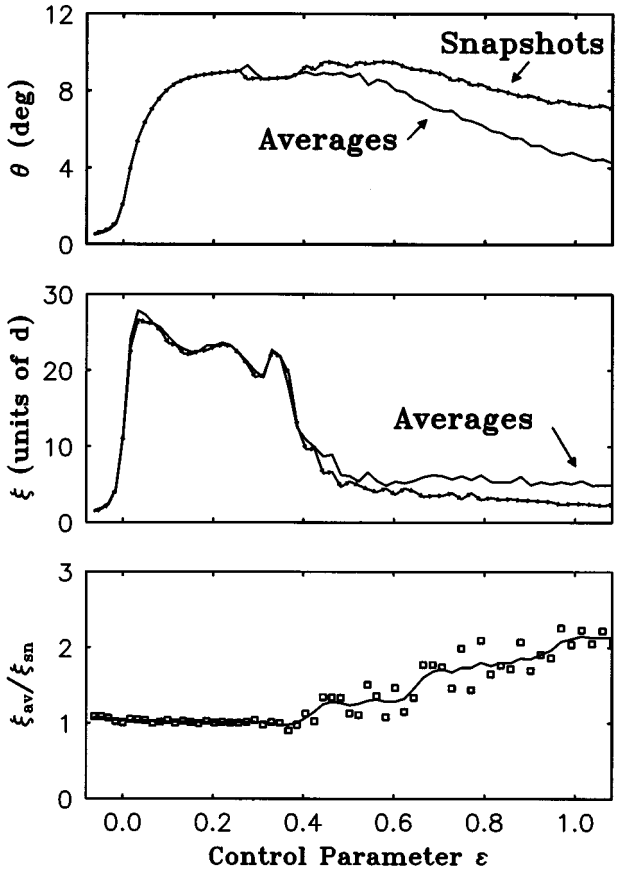

FIG. 13. Order parameter Θ and correlation length ξ of averages and snapshots, taken from the entire digitized image. The averages consists of 64 snapshots, taken 1.3 s apart.

The ratio $\xi_{\mathrm{av}}/\xi_{\mathrm{sn}}$ seems to show several plateaus which we believe to be caused by the box quantization and are due to the fact that we determine the correlation length across the whole convection cell along the x axis. It vanishes when we extract the correlation length from the central regime (96 $\times$96 pixel) of the image (256$\times$256 pixel). The result is shown in Fig. 14.

2. Convergence of averages

In this section we examine how averages arise from snapshots. At a frequency of 10 Hz and a control parameter of $\epsilon=0.66$ we take a data set of 1024 snapshots with a sampling period of 5 s. Because the correlation time is approximately 1.5 s for the chosen control parameter (see Fig. 9), this waiting time ensures that the correlation between two subsequent snapshots is almost zero when considering the assumed Gaussian decay of the temporal autocorrelation. In Fig. 15 we present the amplitude Θ_n and the correlation length ξ_n of the averages as a function of the number of snapshots taken into account.

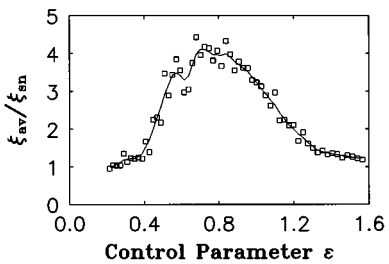

FIG. 14. Ratio of correletion lengths ξ between averages and snapshots, taken from the central regime of the digitized images.

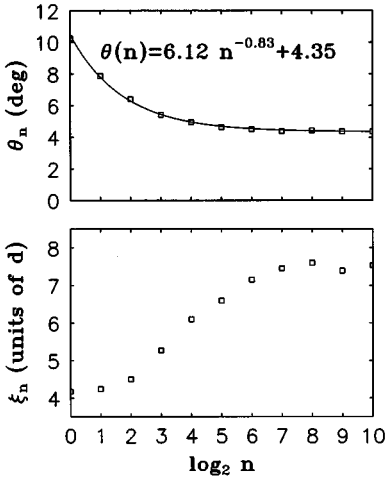

FIG. 15. Order parameter Θ and correlation length ξ of the averages as a function of the amount of snapshots considered.

Precisely speaking, we use 1024 images $K_1^{\mathrm{sn}},\ldots,K_{1024}^{\mathrm{sn}}$, which we divide randomly into m groups of $n=1024/\mathrm{m}$ images. From every group i $(i=1\ldots m)$ we calculate the average image K_i^{av}. Thus each average K_i^{av} consists of n randomly selected snapshots and none of the 1024 snapshots is used twice. Then we calculate the correlation length

$$\xi_n=\frac{1}{m}\sum_{i=1}^{m}\xi(K_i^{\mathrm{av}}),$$

where $\xi(K_i^{\mathrm{av}})$ denotes the correlation length of the average K_i^{av}. The amplitude is calculated in a similar way. So every data point is the result of all 1024 stored images.

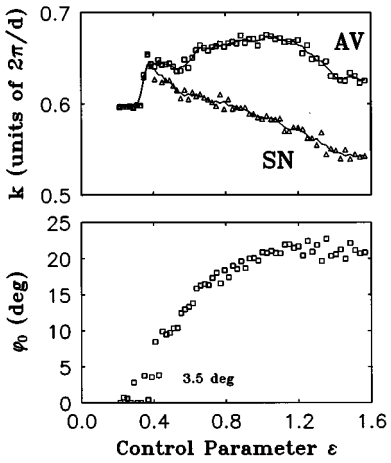

FIG. 16. Upper plot: wave number k of averages and snapshots in the regime of STC, taken from the central regime of the digitized image. Lower plot: estimated angle φ_0 of the oblique structures in the regime of STC.

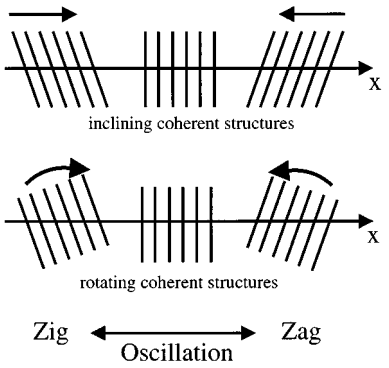

FIG. 17. Illustration of inclining and rotating patches.

The decay of the order parameter Θ_n towards a final value of $\Theta_\infty = 4.35°$ follows a power law with an exponent of about -0.8. This is significantly faster than the convergence rate for a purely stochastic process with an exponent of -0.5.

3. Wave numbers of averages

As shown in Fig. 16, the wave number k_{av} of the averages is systematically larger than the wave number k_{sn} of the snapshots in the regime of STC. The data shown here are taken from the central part of the image as described above. In the following we try to give an explanation for the different wave numbers.

By visual inspection of the pattern, one has the impression of fluctuating coherent structures within the regime of STC. These structures are reminiscent of oblique rolls and seem to oscillate between two states as indicated in Fig. 17. We have made no attempt to quantify this statement. We believe that these structures are a manifestation of the two unstable fixed points corresponding to oblique roll solutions with a finite angle $\pm\varphi > 0$. These oblique rolls are provided by the zigzag instability [17]. Within an infinite system, they are stable [18]. In our system, we do not observe stable oblique rolls, presumably because they create defects at the lateral boundaries and thus lead to STC. If this assumption is correct, a snapshot would be dominated by patches of oblique rolls with the wave number $k_{\mathrm{sn},x}$ because the solution has the highest probability of being in the neighborhood of one of the two unstable fixed points. We speculate that the route from zig to zag is via a rotation of the patch (compare Fig. 17, bottom). The transient normal pattern then has a larger wave number $k_{\mathrm{av},x} = k_{\mathrm{sn},x}\cos\varphi_0^{-1}$ when passing $\varphi = 0$. Because only this pattern is able to match with the lateral boundaries, the averages will consist of this type of pattern.

In Fig. 16 (bottom) we show the angle $\varphi_0 = \arccos(k_{\mathrm{sn},x}/k_{\mathrm{av},x})$. This plot could give a hint about the angle corresponding to the unstable oblique rolls. The figure indicates a quantization of the angle at $\varphi_0 = 3.5°$ that is believed to be caused by the finite-size quantization within the cell.

IV. SUMMARY AND CONCLUSION

In order to quantify recent findings about spatial symmetries in spatiotemporal chaotic patterns, we have performed experiments of electroconvection in cells with a small aspect ratio. After discussing the characteristics of the onset of convection, we presented quantitative results concerning spatiotemporal chaos. We regard a Gaussian decay to be the adequate function to fit spatiotemporal correlations. It turns out that, within the regime of STC, the correlation time decreases with increasing control parameter according to a power law. We are able to quantify the difference between averages and snapshots in terms of our empirical fitting functions. In particular, we have measured amplitudes, wave numbers, correlation lengths, and correlation times. In principle, one could expect a spatial dependence of all these numbers. A systematic survey of those effects is currently under investigation.

ACKNOWLEDGMENTS

It is a pleasure to thank L. Kramer and W. Pesch for enlightening discussions. The experiments were supported by NATO Grant No. CRG 950243.

[1] J. Brindley, K. Kaneko, and T. Kapitaniak, Chaos, Solitons, Fractals **4**, 1193 (1994).
[2] P.C. Hohenberg and M. Shraimar, Physica D **37**, 109 (1989).
[3] R. Benzi, S. Ciliberto, C. Baudet, and G.R. Chavarria, Physica D **80**, 385 (1995).
[4] B.J. Gluckman, C.B. Arnold, and J.P. Gollub, Phys. Rev. E **51**, 1128 (1995).
[5] L. Ning, Y. Hu, R.E. Ecke, and G. Ahlers, Phys. Rev. Lett. **71**, 2216 (1993).
[6] E. Bosch, H. Lambermont, and W. van de Water, Phys. Rev. E **49**, 3580 (1994).
[7] I. Rehberg, B.L. Winkler, M. de la Torre Juárez, S. Rasenat, and W. Schöpf, Adv. Solid State Phys. **29**, 35 (1989).
[8] L. Kramer and W. Pesch, Annu. Rev. Fluid Mech. **27**, 515 (1995).
[9] G. Pfister and I. Rehberg, Phys. Lett. **83A**, 19 (1981).
[10] R. Graham and J.A. Domaradzki, Phys. Rev. A **26**, 1572 (1982).
[11] E. Bodenschatz and L. Kramer, Physica D **27**, 249 (1987).
[12] I. Rehberg, F. Hörner, and G. Hartung, J. Stat. Phys. **64**, 1017 (1991).
[13] Levenberg-Marquard method, taken from W.H. Press, S.A. Teukolsky, W.T. Vetterling, and B.P. Flannery, *Numerical Recipies in C* (Cambridge University Press, Cambridge, 1994).
[14] E. Bodenschatz, W. Zimmermann, and L. Kramer, J. Phys. (Paris) **49**, 1875 (1988).
[15] S. Nasuno, O. Sasaki, S. Kai, and W. Zimmermann, Phys. Rev. A **46**, 4954 (1992).
[16] G. Ahlers, D.S. Cannell, M.A. Dominguez-Lerma, and R. Heinrichs, Physica D **23**, 202 (1986).
[17] M. Kaiser and W. Pesch, Phys. Rev. E **48**, 4510 (1993).
[18] E. Braun, S. Rasenat, and V. Steinberg, Europhys. Lett. **15**, 597 (1991).

[19] L. Kramer and P.C. Hohenberg, Physica D **13**, 357 (1984).
[20] M.C. Cross, P.G. Daniels, P.C. Hohenberg, and E.D. Siggia, J. Fluid Mech. **127**, 155 (1983).
[21] N.B. Tufillaro, R. Ramshankar, and J.P. Gollub, Phys. Rev. Lett. **62**, 422 (1989).
[22] S. Kai and W. Zimmermann, Crystals, Prog. Theor. Phys. **99**, 458 (1989).
[23] S.W. Morris, E. Bodenschatz, D.S. Cannell, and G. Ahlers, Phys. Rev. Lett. **71**, 2026 (1993).